Simple and efficient all-optical production of spinor condensates

J. Jiang,[1] L. Zhao,[1] M. Webb,[1] N. Jiang,[2] H. Yang,[2] and Y. Liu[1,*]
[1]*Department of Physics, Oklahoma State University, Stillwater, Oklahoma 74078, USA*
[2]*Center for Quantum Information, IIIS, Tsinghua University, Beijing, China*
(Received 4 June 2013; revised manuscript received 13 August 2013; published 17 September 2013)

We present a simple and optimal experimental scheme for an all-optical production of a sodium spinor Bose-Einstein condensate (BEC). With this scheme, we demonstrate that the number of atoms in a pure BEC can be greatly boosted by a factor of 5 over some widely used schemes in a simple single-beam or crossed-beam optical trap. Our scheme avoids technical challenges associated with some all-optical BEC methods and may be applicable to other optically trappable atomic species. In addition, we discuss an upper limit for evaporative cooling efficiency in all-optical BEC approaches and a good agreement between our theoretical model and experimental data.

DOI: 10.1103/PhysRevA.88.033620 PACS number(s): 67.85.Hj, 64.70.fm, 37.10.Jk, 32.60.+i

I. INTRODUCTION

In the last two decades, many techniques have been developed to reliably generate a Bose-Einstein condensate (BEC) of more than 10^4 atoms. Almost every one of these techniques requires evaporative cooling in a trapping potential, including a magnetic trap, an optical dipole trap (ODT), or a combined magnetic and optical potential [1–5]. Among these techniques, all-optical methods have been proven to be versatile and popularly applied in producing quantum-degenerate gases of both bosonic [6–14] and fermionic [15] species. ODTs have tight confinement, which allows for fast evaporation with a duty cycle of a few seconds [6]. Unlike magnetic potentials that only trap atoms in the weak-field-seeking spin state, an ODT can confine all spin components. This is crucial for creating vector (spinor) BECs with a spin degree of freedom [16]. ODTs can also be applied to a wider variety of atomic species (e.g., ytterbium, alkaline-earth metals, and cesium) which cannot be feasibly condensed in a magnetic trap [8,13]. In addition, optical trapping does not require magnetic coils around trapped atoms, which not only provides better optical access but also reduces residual magnetic fields. The simplicity and versatility of ODTs widens the accessibility of BEC research on many-body physics, precision measurements, and quantum information science [17].

Forced evaporation in an ODT can be performed by simply reducing its trap depth U (e.g., lowering the trapping laser power). In this process, collision rates decrease with U, which leads to slow rethermalization and eventually stagnation in evaporative cooling. Several methods have been reported to overcome this difficulty, including tilting an ODT with a magnetic-field gradient [18], using a misaligned crossed ODT [12,14], compressing an ODT with a mobile lens [11], and applying multiple ODTs for staged evaporation [8,10]. In this paper, however, we show that these methods may not be necessary for some atomic species, in particular, sodium atoms. Good agreements between our model and experimental data enable us to develop an optimal ODT ramp and evaporation sequence for an all-optical production of sodium BECs. With this optimal scheme, we find that the number of atoms in a pure BEC is greatly boosted by a factor of 5 over some popular schemes and evaporation efficiency $\gamma = -d(\ln D)/d(\ln N)$ can be 3.5 in a crossed ODT. Here D is the phase space density, and N is the number of atoms. We also show an upper limit for γ at a given truncation parameter $\eta = U/k_BT$ and demonstrate that a constant η does not yield more efficient evaporative cooling. Here T is the atom temperature and k_B is the Boltzmann constant. This optimal experimental scheme allows us to avoid technical challenges associated with some all-optical BEC approaches.

II. EXPERIMENTAL SETUP

Our apparatus is divided by differential pumping tubes into an atomic oven chamber, an intermediate chamber, and a main chamber where a magneto-optical trap (MOT) is located [19], as shown in Fig. 1(a). Hot atoms are slowed down by a spin-flip Zeeman slower [21] and then collected in the MOT, which is constructed with six cooling beams and a pair of 24-turn anti-Helmholtz coils. Each MOT cooling beam is detuned by $\delta_{\text{cooling}} = -20$ MHz from the cycling transition, has a power of 6 mW, and combines with one 3.5-mW MOT repumping beam in a single-mode fiber. Every MOT repumping beam is detuned by $\delta_{\text{repump}} = -5$ MHz from the $|F = 1\rangle$ to $|F' = 2\rangle$ transition. After 8.5 s of MOT loading, a three-step polarization gradient cooling process efficiently cools 3×10^8 atoms to 40 μK [19]. To depump atoms into the $F = 1$ hyperfine states, the repumping beams are extinguished 1 ms before cooling beams and MOT coils are turned off. Figure 1(b) lists a typical experimental sequence for our all-optical BEC approach.

A crossed ODT consists of two far-detuned beams which originate from an IR laser with a maximum power of 13 W at 1064 nm and have a waist of 33 μm [22] at their intersection point, as shown in Fig. 1(a). A single-mode polarization-maintaining fiber is used to polish the beam mode and to minimize pointing fluctuations due to imperfections of the IR laser and thermal contractions of an acoustic-optical modulator. As a result, atoms which are transferred from the MOT into the tightly focused crossed ODT demonstrate a long lifetime of 8 s and a large collision rate. These are essential for all-optical BEC approaches.

A couple of ODT ramp sequences were proposed to improve the ODT capture efficiency by finding a reasonable balance between two competing ODT-induced effects [6,7,9,10,12–14,23,24]. First, a larger U enables more atoms to

*yingmei.liu@okstate.edu

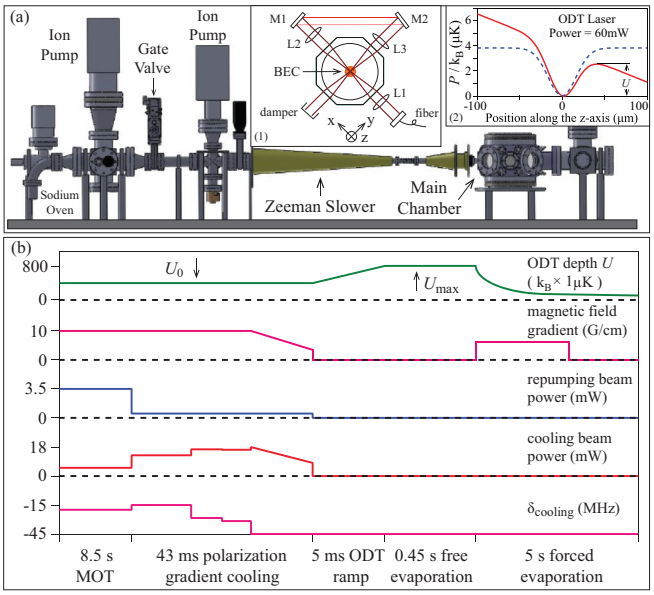

FIG. 1. (Color online) (a) Schematic of our apparatus. Inset 1: schematic of the crossed ODT setup around the main chamber. The positive z axis represents the direction of gravity. L_1, L_2, and L_3 are convex lenses. M_1 and M_2 are mirrors. Inset 2: the definition of the ODT trap depth U. The solid red line and dashed blue line represent the crossed ODT's trap potential energy P as a function of position along the z axis with and without taking into account the influence of gravity, respectively [20]. Here $x = y = 0$ and the ODT laser power is 60 mW. (b). Experimental sequence of creating sodium BECs with the all-optical approach (see text). Each MOT cooling beam is detuned by $\delta_{cooling}$ from the cycling transition. All axes are not to scale.

be captured in the ODT if the ODT beams do not interact with the MOT. The number of atoms loaded in the ODT is $N_{rampA} \sim \int_0^U \rho(\epsilon) f(\epsilon) d\epsilon$, where $\rho(\epsilon)$ and $f(\epsilon)$ are the density of states and occupation number at energy ϵ, respectively. This is confirmed by our data (blue triangles in Fig. 2) taken with

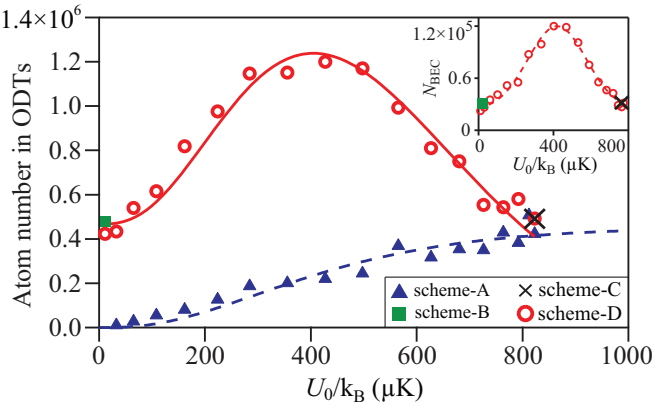

FIG. 2. (Color online) The number of atoms captured in the crossed ODT as a function of U_0 with the four ODT ramp sequences (see text). Our optimal scheme is the best scenario of scheme D when $U_0 \simeq U_{max}/2$. The dashed blue line and the solid red line are fits based on N_{rampA} and N_{rampD}, respectively (see text). Inset: the number of atoms in a BEC as a function of U_0 when one of the three schemes (i.e., schemes B–D) and the same evaporation curve are applied. The dashed red line is a Gaussian fit to the data.

scheme A, in which the ODT depth is linearly ramped in 5 ms from zero to U_0 immediately after MOT beams are switched off. On the other hand, there are some advantages to turning on intense ODT beams in the presence of MOT beams. For example, this allows the ODT to capture a larger number of cold and dense atoms by using MOT beams to prevent the gas from expanding. However, atoms experience non-negligible ac Stark shifts in regions where the ODT beams and the MOT overlap. As a result, the MOT's cooling capability is impaired in the MOT and ODT overlapping regions, and the number of atoms loaded into the ODT decreases when the ODT becomes too deep. N is thus not a monotonic function of U.

Scheme B (green squares in Fig. 2) is a popular scheme used to improve the ODT capture efficiency, in which ODT beams overlap with a MOT for a very short amount of time (20–200 ms) before the MOT beams are switched off [12,14,23,24]. Scheme C (black crosses in Fig. 2) is another widely applied scheme, which keeps the ODT beam at its maximum power during the entire MOT stage [6,9,10,13]. Figure 2 clearly shows that there is an optimal scheme which can increase the number of atoms loaded into the crossed ODT by a factor of 2.5 over the above two popular schemes. This optimal scheme is the best-case scenario for our scheme D. As shown in Fig. 1(b), the ODT in scheme D is kept at a small trap depth U_0 during the entire laser cooling process and is then linearly ramped to U_{max} in $t_{ramp} = 5$ ms. $U_{max} \approx k_B \times 800\ \mu$K is the maximal trap depth used in this work, and $0 \leqslant U_0 \leqslant U_{max}$. The number of atoms loaded into the ODT in scheme D may be expressed as $N_{rampD} \sim A\xi(U_0) \int_0^{U_0} \rho(\epsilon) f(\epsilon) d\epsilon + \int_{U_0}^{U_{max}} \rho(\epsilon) f(\epsilon) d\epsilon$. Here $\xi(U_0) = \exp\{-[\delta_{ODT}(U_0)]^2/\omega_0^2\}$ is a correction factor due to the ODT-induced shift $\delta_{ODT}(U_0)$, while A and ω_0 are fitting parameters. Our data collected with scheme D (red circles in Fig. 2) can be well fitted by this model. The fit value of ω_0 is 1.2Γ, where $\Gamma/2\pi = 9.7$ MHz is the natural linewidth of sodium. The number of atoms in the ODT reaches its peak when the optimal ramp sequence with $U_0 \simeq U_{max}/2$ is applied. Compared to the two popular schemes, the optimal scheme allows us to use ODT beams with smaller waists while loading the same amount of laser-cooled atoms to the ODT. The resulting high initial atom density and high collision rates from the optimal scheme enable very efficient evaporative cooling. This greatly boosts the number of atoms in a BEC by a factor of 5 over the two popular schemes for our apparatus, as shown in the inset in Fig. 2.

We find that our optimal scheme leads to a better ODT capture efficiency over the two popular schemes at every given frequency of the MOT beams within a wide range (i.e., -24 MHz $\leqslant \delta_{cooling} \leqslant -10$ MHz and -15 MHz $\leqslant \delta_{repump} \leqslant 6$ MHz). One mechanism may explain this phenomenon: well-aligned crossed ODT beams have a much larger intensity in the intersection region than that in the "wing" (nonintersecting) region. In other words, the light shift induced by the ODT beams is not uniform, i.e., a big shift in the intersection region and a small shift in the "wing" region. These ODT-induced nonuniform shifts cannot be mimicked by simply varying the frequencies of the MOT cooling and repumping beams. Because this mechanism does not depend on atomic species, our optimal scheme may thus be applicable to rubidium and other optical trappable atomic species.

III. EVAPORATIVE COOLING

To optimize γ, it is necessary to understand the time evolution of the system energy E and the atom number N during an evaporation process. Similar to Refs. [14,25–27], we use $\kappa k_B T \approx (\eta-5)/(\eta-4)k_B T$ to represent the average kinetic energy taken by an atom when it is removed from the ODT, and we assume the mean kinetic energy and mean potential energy to be $E/2$ when η is large. The time evolution of E and N is thus given by

$$\begin{aligned}\dot{E} &= -\frac{2(\eta-4)e^{-\eta}N}{\tau_2}(U+\kappa k_B T)+\frac{\dot{U}}{U}\frac{E}{2}+\dot{E}|_{\rm loss},\\ \dot{N} &= -2(\eta-4)e^{-\eta}N/\tau_2+\dot{N}|_{\rm loss},\end{aligned} \tag{1}$$

where τ_2 is the time constant of the two-body elastic collision. In Eq. (1), $\dot{E}|_{\rm loss}$ and $\dot{N}|_{\rm loss}$ are due to various inelastic loss mechanisms and may be expressed as

$$\begin{aligned}\dot{E}|_{\rm loss} &= k_s N - k_1 N(3k_B T) - k_3 n^2 N(2k_B T),\\ \dot{N}|_{\rm loss} &= -k_1 N - k_3 n^2 N,\end{aligned} \tag{2}$$

where k_1 and k_3 are one-body and three-body loss rates, respectively. k_s represents heating introduced by ODT beams via a number of different mechanisms, such as pointing fluctuations of the ODT beams, a bad laser beam mode, and spontaneous light scattering. The term $2k_B T$ in Eq. (2) accounts for the fact that atoms in the ODT's center have higher density and thus are more affected by the three-body inelastic loss [12].

In our apparatus with the UHV pressure in the 10^{-12} Torr range, background collisions are negligible. Since the ODT beams are delivered via a single-mode polarization-maintaining fiber, heating induced by the ODT beams is minimized. k_1 and k_s are thus very small. If we ignore k_1 and k_s, Eq. (1) can be simplified to

$$\dot{E} = \dot{N}\eta_{\rm eff}k_B T + \frac{\dot{U}}{U}\frac{E}{2}, \tag{3}$$

where $\eta_{\rm eff} = \eta+\kappa-R(\eta+\kappa-2)$. We define $R = (\dot{N}|_{\rm loss})/\dot{N} = 1/[1+2(\eta-4)e^{-\eta}R_{\rm gTb}]$ to represent the portion of atom losses due to inelastic collisions, where $R_{\rm gTb}$ is the ratio of the inelastic collision time constant to τ_2. From solving the above equations, γ may be expressed as

$$\gamma = \eta_{\rm eff}-4 = \eta+\kappa-R(\eta+\kappa-2)-4. \tag{4}$$

The value of η in many publications on optical productions of BECs was held constant with $\Delta\eta = 0$ [6,7,11,12,14,15,18]. Our data in Fig. 3, however, show that a constant η does not lead to better evaporation or a larger γ. The values of γ in Fig. 3 are extracted from 36 evaporation processes in which the forced evaporation speed and the hold time at $U_{\rm max}$ are changed independently, although they all start with the same initial number of cold atoms in the crossed ODT. $\Delta\eta = \eta_{\rm f}-\eta_{\rm i}$ is the change of η during forced evaporation, where $\eta_{\rm i}$ and $\eta_{\rm f}$ are the values of η at $U_{\rm max}$ (i.e., the beginning of forced evaporation) and at $U_{\rm f}$, respectively. In order to avoid overestimating γ due to the bosonic enhancement near the BEC transition temperature, we choose $U_{\rm f} = k_B \times 30\mu$K, where no BEC appears. We find that $\Delta\eta$ tends to be a non-negative value when the forced evaporation time is longer than 1 s (solid black squares in Fig. 3), which is a good indication of sufficient rethermalization. We also find that γ is too small to yield a BEC when $\Delta\eta < -2.5$.

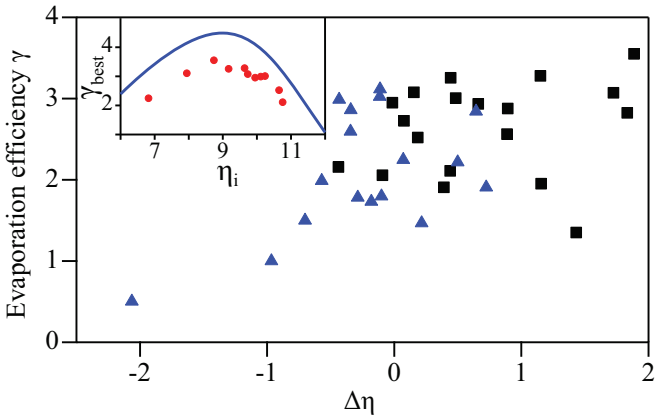

FIG. 3. (Color online) Evaporation efficiency γ in 36 different evaporation processes as a function of $\Delta\eta$. Solid black squares are data taken with the forced evaporation time longer than 1 s. Inset: $\gamma_{\rm best}$ as a function of $\eta_{\rm i}$ extracted from the main figure. The solid line sets an upper limit for γ based on Eq. (4) by assuming $k_1 = k_s = 0$ (see text).

We compare the evaporation efficiency at different values of $\eta_{\rm i}$, as shown in the inset of Fig. 3. $\gamma_{\rm best}$ (the best achieved value of γ at a given η_i in our system) does not show a strong dependence on η_i if $8 < \eta_i < 10$, while $\gamma_{\rm best}$ sharply diminishes when η_i becomes too large or too small. In the inset of Fig. 3, a similar relationship between γ and η_i is also predicted by the solid blue line, which is a result based on Eq. (4) by ignoring k_1 and k_s and by applying a nonzero R (i.e., $R_{\rm gTb} = 4000$ [4]). All of our data lie below the solid line in the inset, which may indicate that k_1 and k_s are larger than zero and cannot be ignored. Therefore, based on Fig. 3, we need to choose a value between 8 and 10 for η_i and keep $\Delta\eta$ larger than -0.5 in order to optimize evaporation efficiency γ.

The maximum achievable value for $\eta_{\rm i}$ appears to be 10.8, as shown in the inset of Fig. 3. To understand this, we monitor the time evolution of η and find that η has a maximal value $\eta_{\rm max}$ at a given ODT depth U. The value of $\eta_{\rm max}$ decreases exponentially with U, and $\eta_{\rm max}$ at $U_{\rm max}$ is 10.8, which agrees well with our theoretical prediction (solid red line in Fig. 4). Therefore, if one wishes to keep η unchanged during forced evaporation, η must be limited to 10.8 even though $\eta_{\rm max}$ can be much higher at low ODT depths (e.g., $\eta_{\rm max} > 13$ for $U/k_B < 100\mu$K). This may be one reason why a constant η does not yield more efficient evaporative cooling. We also find that the time evolution of η at every U discussed in this paper can be well fitted with our model. Two typical fitting curves are shown in the inset of Fig. 4.

A pure $F = 1$ BEC of 1.2×10^5 sodium atoms at 50 nK is created from a 0.45-s free evaporation at $U_{\rm max}$ followed by a 5-s forced evaporation in which U is exponentially reduced. This evaporation curve provides two important parameters for efficient evaporative cooling: η_i is between 8 and 10, and the forced evaporation time is long enough for sufficient rethermalization but short enough to avoid excessive atom losses. Two time-of-flight absorption images in Fig. 5(a) show a typical change in the condensate fraction (CF) after

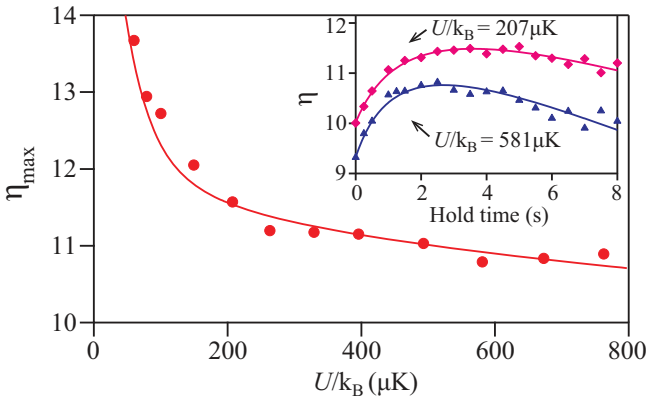

FIG. 4. (Color online) η_{max} as a function of the ODT depth U when atoms are held at a fixed U for 8 s. The solid line is a fit based on Eqs. (1) and (2) (see text). Inset: the time evolution of η at two typical ODT depths. Solid lines are fits based on the same model applied in the main figure (see text).

interrupting the evaporation curve at various U. We also apply the above all-optical approach to evaporate atoms in a single-beam ODT. A similar result can also be achieved in the single-beam ODT as long as its beam waist is smaller than 16 μm so that it can provide a high enough collision rate. The resulting number of condensed atoms in the single-beam ODT, however, is four times smaller than that in the crossed ODT.

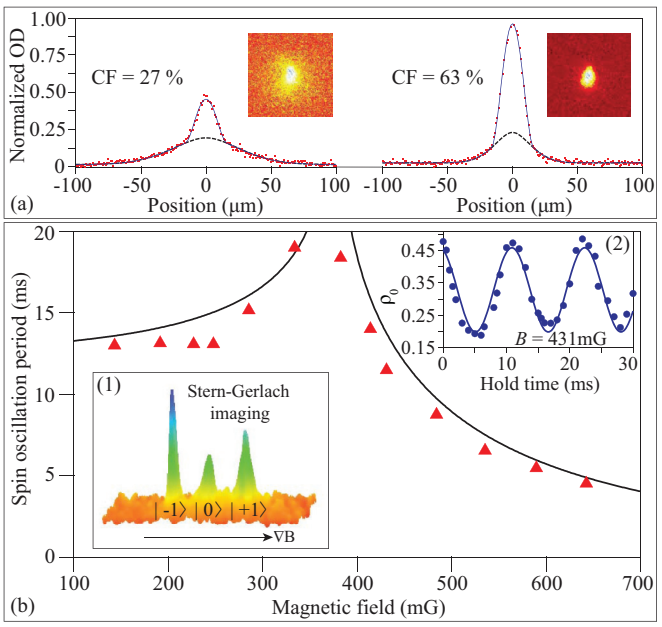

FIG. 5. (Color online) (a) Absorption images taken after interrupting an optimized evaporation curve at various U followed by a 10-ms time of flight (see text). OD stands for the optical density. Dashed black lines and solid blue lines are fits to the column densities based on a Gaussian distribution and a bimodal distribution, respectively. $CF = \tilde{n}_c/(\tilde{n}_{th} + \tilde{n}_c)$, where $\tilde{n}_{th}$ and $\tilde{n}_c$ are column densities for the thermal cloud and the condensate, respectively. (b) The period of spin population oscillations as a function of B at $m = \rho_{+1} - \rho_{-1} = 0$. Here ρ_{m_F} is the fractional population of the m_F state. The solid black line is a fit based on the mean-field theory (see text). Inset 1: Three spin components of a $F = 1$ spinor BEC are spatially separated in a 3D Stern-Gerlach absorption image. Inset 2: A typical time evolution of ρ_0 at $B = 431$ mG and $m = 0$ when the spinor BEC is held in the crossed ODT. The solid blue line is a sinusoidal fit to the data.

To fully polarize atoms in a $F = 1$ BEC to the $|F = 1, m_F = 1\rangle$ state, a weak-magnetic-field gradient is applied during forced evaporation, as shown in Fig. 1(b). We then ramp up a magnetic bias field with its strength B between 100 and 700 mG while turning off the field gradient. We can prepare an initial state with any desired combination of three m_F states by altering the amplitude and duration of a resonant rf pulse and/or a resonant microwave pulse. A Stern-Gerlach separation followed by absorption imaging is used to measure the populations of different spin states, as shown in inset 1 in Fig. 5(b).

The interesting interactions in spinor BECs are interconversion among multiple spin states and magnetic-field interactions characterized by the quadratic Zeeman effect. Such a system can be described with a simple two-dimensional phase space that we can manipulate to some degree by changing the magnetic-field strength or the density of the BEC [17,28]. When a $F = 1$ spinor BEC is taken out of equilibrium at a nonzero magnetic field, spin population oscillations can be observed, as shown in inset (2) in Fig. 5(b). The population oscillations are nearly harmonic except near $B = 370$ mG, a separatrix in phase space where the period diverges. The data can be well fitted by a prediction from the mean-field theory [solid line in Fig. 5(b)] [17] with only one fitting parameter (i.e., the mean BEC density). Figure 5(b) may thus be a good way to measure the mean BEC density and to check the values of the crossed ODT's trap frequency and trap depth [22].

IV. CONCLUSION

In conclusion, we have presented an optimal experimental scheme for an all-optical production of sodium spinor BECs. For our apparatus, we have found that the number of atoms in a pure BEC with this scheme is greatly boosted by a factor of 5 over two popular schemes in a crossed ODT. Our scheme avoids technical challenges associated with some all-optical BEC approaches and may be applicable to other optically trappable atomic species and molecules [29]. We have showed an upper limit for γ at a given η, demonstrated that a constant η could not yield a larger γ, and discussed good agreements between our model and experimental data. We may be able to further improve evaporation efficiency to reach its upper limit and thus to increase the number of atoms in a BEC by combining our scheme with one of the clever ideas shown in [8,12,14,18].

ACKNOWLEDGMENTS

We thank the Army Research Office, Oklahoma Center for the Advancement of Science and Technology, and Oak Ridge Associated Universities for financial support. M.W. thanks the Niblack Research Scholar program. N.J. and H.Y. thank the National Basic Research Program of China.

[1] K. B. Davis, M.-O. Mewes, M. R. Andrews, N. J. van Druten, D. S. Durfee, D. M. Kurn, and W. Ketterle, Phys. Rev. Lett. **75**, 3969 (1995).
[2] M. H. Anderson, J. R. Ensher, M. R. Matthews, C. E. Wieman, and E. A. Cornell, Science **269**, 198 (1995).
[3] C. C. Bradley, C. A. Sackett, J. J. Tollett, and R. G. Hulet, Phys. Rev. Lett. **75**, 1687 (1995).
[4] W. Ketterle and N. J. van Druten, Adv. At. Mol. Opt. Phys. **37**, 181 (1996).
[5] Y.-J. Lin, A. R. Perry, R. L. Compton, I. B. Spielman, and J. V. Porto, Phys. Rev. A **79**, 063631 (2009).
[6] M. D. Barrett, J. A. Sauer, and M. S. Chapman, Phys. Rev. Lett. **87**, 010404 (2001).
[7] R. Dumke, M. Johanning, E. Gomez, J. D. Weinstein, K. M. Jones, and P. D. Lett, New J. Phys. **8**, 64 (2006).
[8] T. Weber, J. Herbig, M. Mark, H.-C. Nägerl, and R. Grimm, Science **299**, 232 (2003).
[9] C. S. Adams, H. J. Lee, N. Davidson, M. Kasevich, and S. Chu, Phys. Rev. Lett. **74**, 3577 (1995).
[10] K. J. Arnold and M. D. Barrett, Opt. Commun. **284**, 3288 (2011).
[11] T. Kinoshita, T. Wenger, and D. S. Weiss, Phys. Rev. A **71**, 011602 (2005).
[12] J.-F. Clément, J.-P. Brantut, M. Robert-de-Saint-Vincent, R. A. Nyman, A. Aspect, T. Bourdel, and P. Bouyer, Phys. Rev. A **79**, 061406 (2009).
[13] Y. Takasu, K. Maki, K. Komori, T. Takano, K. Honda, M. Kumakura, T. Yabuzaki, and Y. Takahashi, Phys. Rev. Lett. **91**, 040404 (2003).
[14] A. J. Olson, R. J. Niffenegger, and Y. P. Chen, Phys. Rev. A **87**, 053613 (2013).
[15] S. R. Granade, M. E. Gehm, K. M. O'Hara, and J. E. Thomas, Phys. Rev. Lett. **88**, 120405 (2002).
[16] J. Stenger, S. Inouye, D. M. Stamper-Kurn, H.-J. Miesner, A. P. Chikkatur, and W. Ketterle, Nature (London) **396**, 345 (1998).
[17] D. M. Stamper-Kurn and M. Ueda, Rev. Mod. Phys. **85**, 1191 (2013).
[18] C.-L. Hung, X. Zhang, N. Gemelke, and C. Chin, Phys. Rev. A **78**, 011604 (2008).
[19] The intermediate chamber allows us to refill alkali metals and get UHV pressures back to the 10^{-12} Torr range within 24 h. The first polarization gradient cooling step compresses the MOT for 20 ms by increasing the power of each cooling beam to 12 mW while changing δ_{cooling} to -15 MHz. In this step, the power of each MOT repumping beam is also drastically reduced to 45 μW. Then during a 5-ms premolasses step, every cooling beam is further red detuned in addition to its power being increased to 16 mW. This is followed by a 18-ms optical molasses, in which a cooling beam is detuned to $\delta_{\text{cooling}} = -45$ MHz and its power linearly drops to 8 mW. The magnetic-field gradient is also reduced to 3 G/cm over the 18 ms.
[20] The crossed ODT trap potential energy is $P = P_1 + P_2 + P_g$, where P_1 and P_2 are trap potentials of the two single-beam ODTs and P_g is due to the influence of gravity.
[21] L. Zhao, J. Jiang, J. Austin, M. Webb, Y. Pu, and Y. Liu (unpublished).
[22] We determined the value of the ODT's beam waist by measuring its trap frequency with two methods. First, we recorded the number of atoms in the ODT after sinusoidally modulating U at various modulation frequencies f_{m}. The number of atoms exhibits parametric resonances at $f_{\text{m}} = l f_{\text{ODT}}$, where f_{ODT} is the ODT's radial frequency and l is a positive integer number. In the second method, we kicked atoms in the single-beam ODT with a magnetic-field gradient and then recorded the position of atoms after holding the atoms in the ODT for a variable length of time. It appeared that atoms experienced a harmonic oscillation with a frequency equal to the ODT's axial frequency. We ensured the two ODT beams were well intersected at their focal points with high-resolution imaging in three orthogonal directions. The values of the ODT's beam waist and its trap depth provided by these two methods are very close to each other and also agree with those derived from Fig. 5(b). In this paper, the uncertainty of η is found to be $\sim$4% based on the measurements with the above three methods.
[23] S. J. M. Kuppens, K. L. Corwin, K. W. Miller, T. E. Chupp, and C. E. Wieman, Phys. Rev. A **62**, 013406 (2000).
[24] T. Takekoshi and R. J. Knize, Opt. Lett. **21**, 77 (1996).
[25] K. M. O'Hara, M. E. Gehm, S. R. Granade, and J. E. Thomas, Phys. Rev. A **64**, 051403 (2001).
[26] O. J. Luiten, M. W. Reynolds, and J. T. M. Walraven, Phys. Rev. A **53**, 381 (1996).
[27] M. Yan, R. Chakraborty, A. Mazurenko, P. G. Mickelson, Y. N. Martinez de Escobar, B. J. DeSalvo, and T. C. Killian, Phys. Rev. A **83**, 032705 (2011).
[28] Y. Liu, S. Jung, S. E. Maxwell, L. D. Turner, E. Tiesinga, and P. D. Lett, Phys. Rev. Lett. **102**, 125301 (2009).
[29] Upon completion of this work, we recently become aware of Ref. [30] and its ODT ramp sequence, which linearly ramps ODTs from $U_{\text{max}}/3$ to U_{max} in $t_{\text{ramp}} = 2$ s. We find that the number of atoms in a pure BEC exponentially decreases with t_{ramp} when $t_{\text{ramp}} > 0.01$ s in our system. The optimal sequence explained in our paper yields a pure BEC of at least twice the number of atoms as that from a sequence with $t_{\text{ramp}} = 2$ s for our apparatus.
[30] D. Jacob, E. Mimoun, L. D. Sarlo, M. Weitz, J. Dalibard, and F. Gerbier, New J. Phys. **13**, 065022 (2011).